Chapter 2

Ferrite Nanostructures Consolidated by Spark Plasma Sintering (SPS)

Romain Breitwieser, Ulises Acevedo, Souad Ammar and Raul Valenzuela

Additional information is available at the end of the chapter

http://dx.doi.org/10.5772/68017

Abstract

Ferrites are a well-known class of ferrimagnetic materials. In the form of nanoparticles (NPs), they exhibit novel and fascinating properties, leading to an extremely wide variety of applications in electronics, biomedical and environmental fields. These applications result from nanoscale effects on physical properties, particularly magnetic properties. For applications in electronic devices, however, a high-density, consolidated body, with very fine grains is needed, in order to retain the nanoscale properties. To our knowledge, spark plasma sintering (SPS) is the only method permitting a full densification with final grain size in the nanometer range. In this review, we examine the SPS method as applied to ferrites and, in particular, the effects of SPS parameters on the final nanostructures obtained. Due to their technological impact, we also discuss the SPS fabrication of hybrid multiferroic nanostructures composed of a ferrite and a ferroelectric phase.

Keywords: spark plasma sintering, ferrites, nanostructures

1. Introduction

Ferrite materials have been widely used because of their excellent magnetic and electric properties. With three basic crystal structures, spinel, garnet and hexagonal unit cells, they can form a virtually endlessly number of solid solutions and thus be tailored for most applications [1]. Ferrite-based devices [2] are used in all communication systems (magnetic storage, microwave absorbers, high frequency inductors, radar devices, phase array antennas), different electric motors (a modern car has more than 30 DC motors), as permanent magnets. Hexagonal ferrites still constitute about 75% of the permanent magnet world market [3].

Developed since the 1930s, ferrites are sometimes considered as a "mature" technology, with the implication that advances in this field would only be incremental. This, in fact, is very far from reality [4]. A simple look at specialized literature shows that advances in ferrite processing and devices during the last 10 years have been dramatic and significant.

The ferrite size reduction from bulk to nanoscale has opened a whole new field of potential applications, as well as many issues on basic research. Magnetic properties of nanoparticles can be quite different [5] from those of their microsized or bulk counterparts. As the dimensions are reduced below a critical size, magnetic properties change from those of multidomain to those of single domain structure. Magnetic moments at the particle surface become noncollinear due to broken exchange bonds at the external layer of the particles. An additional complexity arises from the interactions (dipolar, exchange) between particles, a subject which so far, has been poorly understood. The macroscopic magnetic properties of nanoparticle-based materials can be therefore extremely complex. But as it occurs very often, a source of complexity can become also a source of novel applications and knowledge once properly understood.

Nanoferrite technology has been ongoing for the last 20 years, with recent advances in magnetic fine particle production by many innovative routes. However, for most applications in electronic devices, a nanoparticle powder is unsuitable; a high density and fully consolidated material is needed. Conventional sintering–usually operated at temperatures in excess of 1100°C for a few hours–leads to an excessive grain growth, making such a method unacceptable to consolidate nanoscale materials.

A novel sintering technique has been recently developed in Japan, known as spark plasma sintering (SPS) [6], consisting of generating internally heat by means of DC current pulses directly through a graphite die containing the powder compact. This technique allows very fast heating and cooling rates (up to 1000°C/min) and has shown its potential to consolidate nanoparticle powders into high-density samples with controlled grain growth. Contrary to conventional sintering, ferrites have been consolidated to high density at temperatures as low as 500°C with sintering times as short as 5 min, while keeping grain size in the 100 nm range [7].

Recently, SPS has also shown [8, 9] the capability to consolidate nanohetero-structures in order to fabricate multifunctional materials of strong scientific and technological interest. Typically, ferrites combined with ferroelectric perovskites may lead to extrinsic multiferroics in which the magnetization of the former can be driven by the application of an electric field and vice-versa. The efficiency of this magnetoelectric exchange depends critically on the morphology of interfaces [10, 11], which in turn is controlled by the SPS process parameters.

In this chapter, we present a review of nanostructures that have been obtained by means of SPS. In Section 2, a self-contained review of the basic aspects of ferrites is given. Section 3 describes the main features of the spark plasma sintering method. The methods to synthesize ferrite NPs that can be used as precursors for the subsequent SPS consolidation are briefly described in Section 4. A review of results obtained on spinel ferrites using SPS is given in Section 5. The consolidation of ferrites with garnet and hexagonal unit cells is discussed in Sections 6 and 7, respectively. Section 8 describes the application of SPS to the fabrication of ferrite-based multiferroic composites, and a general conclusion is given in Section 9.

http://dx.doi.org/10.5772/68017

2. Overview of crystal structure and magnetic properties of ferrites

2.1. Spinels

Spinel ferrites possess the crystal structure of the natural spinel $MgAl_2O_4$, where Mg and Al have been substituted by transition cations. This structure is particularly stable, and there is a large variety of oxides which adopt it, fulfilling the conditions of overall cation-to-anion ratio of 3/4, a total cation valence of 8. An important ferrite is magnetite, $Fe^{2+}Fe^{3+}{}_2O_4(Fe_3O_4)$, the oldest known magnetic solid which is still being researched due to the fascinating properties associated with the coexistence of ferrous and ferric cations. Another important ferrite material is maghemite or γ-Fe_2O_3, which is a defective spinel $Fe^{3+}{}_{8/3}\square_{1/3}O_4$, where □ represents vacancies on octahedral cation sites. The cation distribution, that is, the occupancy of sites by cations depends on many parameters [1] such as ion size, valence, electronic symmetry, and even cooling rate when they are prepared by sintering, which is the most frequently used process. When divalent cations occupy tetrahedral (or "A") sites and trivalent ones are on octahedral (or "B") sites, it is known as a normal spinel. A different cation distribution, where half of trivalent cations occupy A sites and B sites, is shared by divalent cations and the remaining trivalent cations are known as the inverse spinel. An intermediate cation distribution has been obtained for some ferrites, where cations are statistically distributed on the two sites.

A remarkable characteristic of spinel structure is that it is able to form an extremely wide variety of solid solutions by the partial or total substitution of divalent, or trivalent cations, leading to an extremely wide diversity of magnetic properties. Magnetic transition temperature, for instance, varies from 9 K for $ZnFe_2O_4$ to –958 K for $Li_{0.5}Fe_{2.5}O_4$ [1].

2.2. Garnets

Magnetic garnets possess the crystal structure of mineral $Mn_3Al_2Si_3O_{12}$, with rare-earth (RE) and Fe^{3+} cations instead, leading to the general formula $RE_3Fe_5O_{12}$, RE is in the series from La^{3+} to Lu^{3+}. The garnet unit cell includes 160 atoms; rare-earth cations occupy dodecahedral sites, and iron cations are distributed among the tetrahedral (three) and octahedral (two) sites. An additional case is yttrium iron garnet, known as "YIG", $Y_3Fe_5O_{12}$, which can be prepared as a very homogeneous phase and exhibits remarkable magnetic properties, especially at microwave frequencies.

As in the case of spinels, cations can be partially or totally substituted to obtain a large number of compositions. Also, as in spinels, magnetic interactions are of the superexchange type. Rare-earth and octahedral magnetic sublattices are oriented parallel and opposite to tetrahedral sublattice. The spontaneous magnetic moments in rare-earth cations are localized in orbital 4*f*, which is an internal one; additionally, dodecahedral sites are very large. These two factors lead to a diminished superexchange interaction, which decreases rapidly with increasing temperature. The main results are that all rare-earth magnetic garnets exhibit virtually the same Curie temperature (560–573 K), as well as a "compensation temperature" where magnetization vanishes due to the mutual compensation of sublattice magnetic moments, and which depends on the rare-earth cation [1].

2.3. Hexaferrites

Hexaferrites are a "family" of hexagonal (and some rhombohedral) closely related structures. The main formulae can be written as follows: $BaFe_{12}O_{19}$ (*M*), $Ba_2Me_2Fe_{12}O_{22}$ (*Y*), $BaMe_2Fe_{16}O_{27}$ (*W*), $Ba_2Me_2Fe_{28}O_{46}$ (*X*), $Ba_4Me_2Fe_{36}O_{60}$ (*U*) and $Ba_6Me_{24}Fe_{48}O_{82}$ (*Z*). Me represents a divalent cation such as Zn, Cu, Mg, Co and Mn. Ba can also be substituted totally or partially by Ca, Sr, Pb. Hexagonal ferrites lead to an extremely wide variety of compositions and hence magnetic properties. Their magnetic structures are quite complex; for example, in the *M* structure, the magnetization results from interaction between five sublattices coupled by superexchange interactions. Hexaferrites are used mostly as permanent magnets due to their hard magnetic properties.

2.4. Magnetic properties of ferrite nanoparticles

The nanoscale adds a complexity level to the magnetic properties of materials [12]. Most of the critical lengths for magnetic properties and structures fall in the nanometer range. Two of the most important changes are the transition from multidomain to single domain and then the change from the long-range ordered ferrimagnetic to the superparamagnetic (SPM) behavior. The former occurs when a nanoparticle (NP) becomes very small, and the energy to produce a domain wall is larger than the magnetostatic energy produced by a single domain configuration. A single domain structure is usually characterized by a maximum on the coercive field. If the size of the particles is still decreased, then the coercive field and the remanent magnetization can vanish as SPM state takes place. Superparamagnetism [5] appears when the particle is very small, and its total anisotropy energy E_K ($E_K = K \cdot V$, with K = anisotropy constant and V = particle volume) is smaller than the thermal energy $E_T = k_B \cdot T$ (with k_B = Boltzmann constant and T = temperature). Thermal energy thus overcomes anisotropy, and the magnetization oscillates randomly. The main difference with the classic paramagnetic behavior is that in the case of SPM, it is the whole magnetization vector which exhibits random reversals, instead of the individual spins. Magnetization, that is, spins coupling is maintained up to the Curie point, T_C.

Since anisotropy energy usually *decreases* with temperature, and thermal energy *increases* with T, there exists a "blocking" temperature, T_B, for which $E_K = E_T$; below this point NPs behave as ordered ferromagnetic (anisotropy dominates), and above T_B, NPs become superparamagnetic, with random magnetization.

Superparamagnetism is catastrophic for materials intended for magnetic recording, since any information (in the form of a particular magnetic domain structure) is lost at room temperature. For medical applications, however, SPM is just the magnetic behavior needed. In cancer tumor removal techniques, magnetic NPs (conveniently functionalized) are injected into the patient to be selectively localized onto the tumor. Single domain ferromagnetic NPs, due to their magnetostatic fields, can become aggregated and form large clusters. Once the tumor is eliminated, magnetic NPs can be easily recovered with a magnet because under the effect of a magnetic field, SPM NPs acquire a significant magnetization and are attracted.

http://dx.doi.org/10.5772/68017

The consolidation of NPs by SPS leads to the formation of a polycrystalline structure with grains separated by grain boundaries and the tendency to grain growth. Both of them strongly decrease the surface effects observed in NPs. Magnetic properties can therefore exhibit dramatic changes as compared with the properties of original NPs powder; typically, saturation magnetization increases to approach the bulk value, and coercive field shows a definite value (and thus a remanent magnetization). An interesting case is cobalt ferrite, which can be synthesized as fine NPs in the 5–10 nm range [13]. For such small NPs, cobalt ferrite shows a SPM behavior at room temperature, as in **Figure 1(a)**. Zero-field-cooled, field-cooled (ZFC-FC) experiments usually lead to a blocking temperature in the 100–150 K range (**Figure 1(b)**). Below this T_B, a normal ferromagnetic behavior is observed; at higher temperatures, the anisotropy is overwhelmed by thermal agitation and a SPM phase is observed. However, when these NPs are consolidated by SPS, a typical hysteresis loops with well-defined coercivity and remanence are observed at all temperatures (below the Curie point), as shown in **Figure 1(c)** [14].

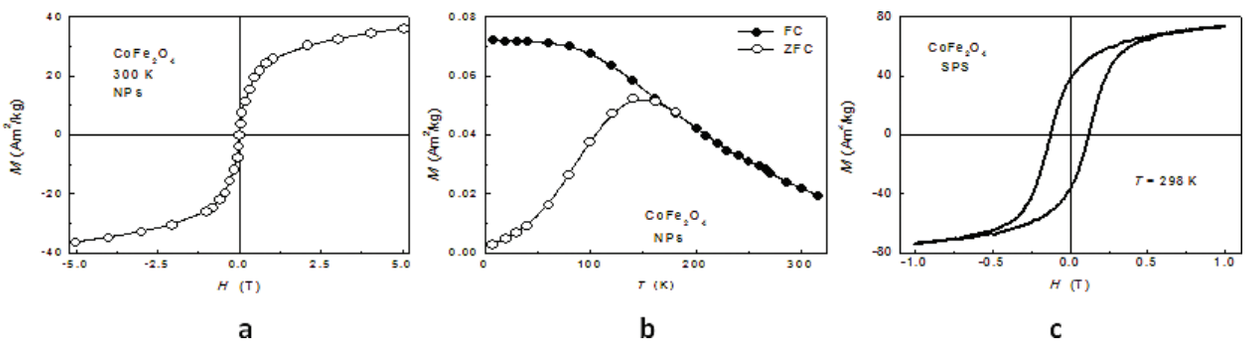

Figure 1. (a) SP behavior of cobalt ferrite NPs in the 10 nm diameter range; (b) magnetization behavior in ZFC-FC measurements, showing a blocking temperature ca. 150 K; and (c) magnetic hysteresis of consolidated sample at 500°C for 5 min (adapted from Refs. [13, 14]).

3. The spark plasma sintering process

In the SPS process, the sample (typically a powder) is placed in graphite die and then compressed by two pistons, **Figure 2**. The heating is by Joule effect, by electric current pulses. High currents (up to 1500 A) and strong pressures (up to 120 MPa with graphite dies and up to 600 MPa with tungsten carbide dies) can be applied, which allow significantly large heating rates (up to 1000°C/min). It is a versatile technique with many processing parameters: sintering temperature T_s, heating and cooling rates (*Hr*, *Cr*, respectively), maximum load (P_s), load rate *Pr*, load removal rate (*Pc*). By measuring the distance between pistons (Z) and its more sensitive time derivative (d*Z*/d*t)* during the process, an estimation of the density changes is recorded, which has a direct relationship with sintering. A typical temperature and shrinkage profile are shown in **Figure 2**. The main objective of the process is to transform a particle powder into a high density solid. In some cases, a chemical reaction can occur during the process, in addition to densification; in this review, only the densification process is discussed.

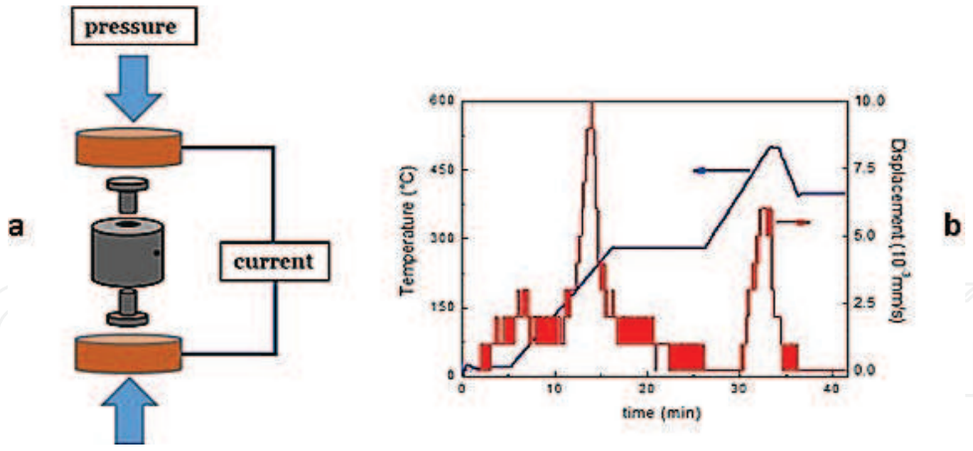

Figure 2. (a) SPS electrodes and die set up; (b) a typical temperature profile (left axis), and shrinkage trace (right axis), in the form of time derivative d*Z*/d*t* for a spinel ferrite (adapted from Ref. [7]).

The densification process, that is, the removal of porosity (corresponding to empty spaces between the original particles) requires diffusion; this is produced, of course, by increasing the temperature. It appears, however, that electric current pulses have an effect also on atomic diffusion, since high densities can be reached at very low temperatures and extremely short times as compared with classic sintering processes. This additional effect of current has been attributed to an increase in point defect concentration [15], as well as a reduction in the activation energy for mobility of defects [16]. In the case of insulators, it appears that it is the electric field that leads to such enhanced diffusion since these materials can also be effectively consolidated by SPS.

The heating rate can have a strong effect on the final microstructure of the material. During the process, there is a competition between densification and grain growth (or "coarsening"). The former, which is basically the removal of porosity, depends on volume diffusion, while grain growth is controlled essentially by surface diffusion. Volume diffusion involves mass transport and hence occurs at higher temperatures than surface diffusion. A high heating rate therefore can "bypass" the range of grain growth alone and start readily the densification with limited coarsening. The possibility to separate these two mechanisms makes SPS the ideal, and so far, the only suitable process to fabricate full density nanostructured materials.

The pressure has a significant influence on final density. At relatively low temperatures, an increase in pressure leads to higher densities. At high temperatures, the increase in density is accompanied by an increase also in grain size. A measure of the shrinkage rate [17] can be obtained from the time derivative of distance between pistons, d*Z*/d*t*, which is directly obtained in most SPS available systems.

4. Brief review of synthesis methods for ferrite nanopowders

To date, a variety of synthetic methods have been applied to produce magnetic nanoparticles, including those of ferrites. These methods can be divided into two main approaches,

http://dx.doi.org/10.5772/68017

a top down and a bottom up ones. Bottom-up routes are attractive in terms of their low cost and sustainability; there is, however, a generic challenge in directly obtaining particles with a calibrated size and a uniform shape. They mainly consist on a direct precipitation of the desired phase starting from selected precursors dissolved for an adjusted atomic ratio in a given solvent and heated at a high enough temperature. The involved reactions depend on the operating conditions: hydrolysis [9, 13], thermal decomposition [18, 19] and condensation.

In some cases, the synthesis is indirect and an intermediate solid phase, like an alcoholate, a hydroxide or a hydroxycarboxylate, is first obtained and then calcined at moderated heating conditions (less than 800°C for a couple of hours in air) in order to form the target phase (see for instance [20, 21]).

The heating conditions of the reaction solution in all these wet chemical methods can be conventional or microwave assisted [22, 23]. They can be achieved under standard pressure or under autogenous pressure (solvothermal route [24–27]). The synthesis can be achieved under high intensity ultrasounds (sonochemical technique [28]) or under energetic radiation (radiolysis method [29, 30]). Surfactants or polymers can be introduced in the reaction medium to improve the control of the size and the shape of the particles and/or to avoid their aggregation.

The top-down method is based on an energetic milling process of a powder [31]. The powder can be the commercial bulk ferrite phase or a mixture of the raw oxide or hydroxides of the metallic cations constituting its composition. The milling process can be carried out using different apparatus, namely attritor, planetary mill or a linear ball milling (**Figure 3**) but in all the cases, the introduced powders are cold welded and fractured during mechanical alloying, favoring in one case its nanostructuration and its chemical reactivity [32, 33].

For all nanocrystalline materials prepared by high-energy ball milling synthesis route, less-effective size control, surface and interface contamination and amorphization are major concerns. In particular, mechanically attributed contamination by the milling tools (Fe, WC, etc.) is often the problem. Recently, surfactant-assisted ball milling has been exploited for the synthesis of various nanomaterials, nanograins, and nanocomposites from solid bulk materials.

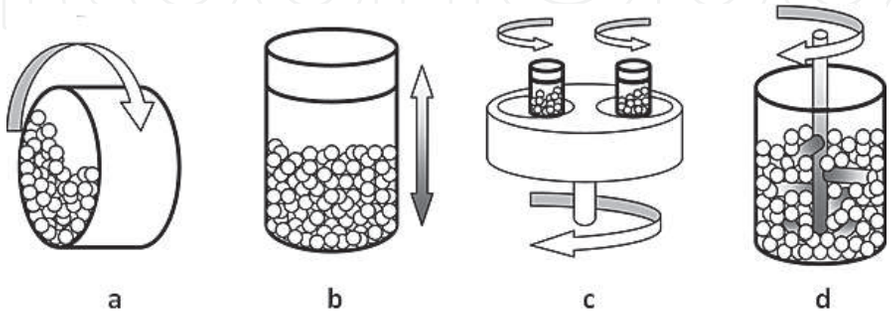

Figure 3. Schematic representation of (a) the indirect direct milling equipment, including (b) linear and (c) planetary mill equipment and that of the direct one (d), called attritor. Republished with permission of the Royal Society of Chemistry, from Ref. [34]; permission conveyed through Copyright Clearance Center, Inc.

Promising results have been obtained in terms of nanostructure assembly, micro-/nanoenvironment, surface functionalities, and dispersion [35].

Focusing on spinel ferrites, all these approaches were successfully used to produce nanoparticles. For instance, cobalt ferrite particles having different sizes were prepared from 2 to 50 nm by sol-gel method [20] and from 2 to 10 nm by polyol process [7, 9, 13, 14, 36], without using any additional capping agents/surfactants. In these cases, the particle size was varied by controlling the temperature of the calcination of the precipitated intermediate solid and that of the heating reaction solution, respectively. As this temperature is elevated, the size of the resulting particles is large, and their crystalline quality is high (see for instance [37–40]). Moreover, such nanoparticles can exhibit a deviation from the thermodynamic spinel stable structure. This deviation, mainly consisting on a change in the cation occupancy of spinel sites, increases with temperature.

By opposition, garnets and hexaferrites nanopowders can be scarcely produced directly. Whatever the employed synthesis route, wet chemistry or ball-milling, the total processing route often involves a subsequent annealing step in order to obtain highly crystallized and pure perovskite or hexagonal phases. For instance, nanostructured M-type $SrFe_{12}O_{19}$ hexaferrite powder was produced by combining forced hydrolysis in polyol followed by subsequent annealing at 836°C [41]. It was also successfully prepared by combining ball milling followed by annealing at 700°C [42]. This annealing step makes the resulting nanopowders typically polycrystalline of several tens of nanometers in crystal size with a magnetization relatively close to that measured on their bulk counterparts. The situation is almost the same for nanostructured garnets. Annealing is required after ball-milling [43] or after sol-gel precipitation [44] for YIG preparation. In some cases, the precursors from these reactions can be used not only for SPS sintering but also for "reactive" SPS treatment, which include the chemical reaction.

5. Consolidation of spinel ferrites by SPS

In a typical SPS powder consolidation experiment, the starting powder is put in the electrically conductive toroidal die made of graphite, and uniaxially pressed by the upper and lower graphite punches. Most of the electric current flows through the mould, and specimen is heated up by Joule effect. The electric current can also flow through the powder materials itself, and self-heating occurs at the inside of the sample. Low temperature and short time sintering are therefore possible. In the case of spinel ferrites, this technique was first used to reduce sintering time on micrometer-sized powders [45, 46]. Then, it was used to reduce the sintering temperature using nanometer-sized powders [7, 9, 47–49].

Spinel nanoferrites were readily synthesized by soft chemistry methods (see Section 3) in a wide variety of compositions and can be directly consolidated by SPS. Ni-Zn ferrites have been consolidated at temperatures as low as 350°C for 10 min, to densities about 85% [50]. Density and grain size increased by increasing the sintering temperature to 400 and 500°C, as appears in **Figure 4**.

http://dx.doi.org/10.5772/68017

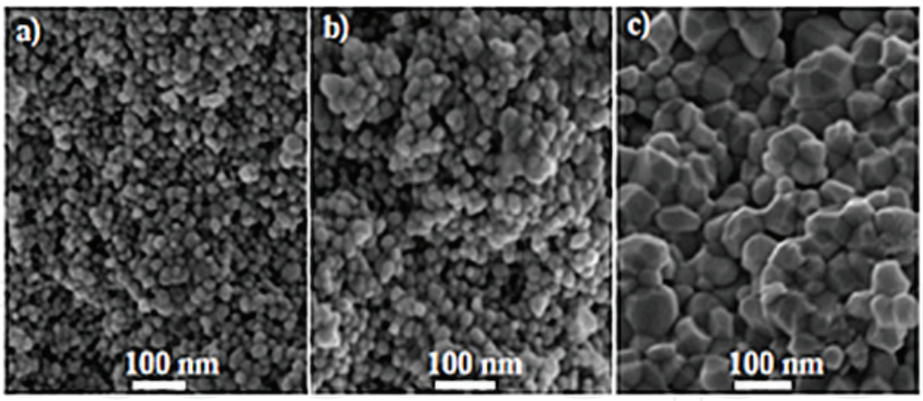

Figure 4. Nanostructures produced by consolidation of Ni-Zn NPs by SPS by 10 min at (a) 350°C, (b) 400°C, and (c) 500°C [51].

Magnetite can be consolidated by SPS into a high density, high crystallinity solid at 750°C for 15 min, with a final grain size in the 150 nm range [49], as shown in **Figure 5(a)**. The reductive atmosphere of SPS prevented the oxidation of initial magnetite NPs to maghemite, γ-Fe_2O_3, first, and then to hematite, α-Fe_2O_3. The quality of the crystals can be assessed by means of the resolution of the Verwey transition [52], which occurs about 120 K in two steps: first the crystallographic transition [53] from the monoclinic to the cubic system and then the spin reorientation from uniaxial to cubic symmetry [54], as shown in **Figure 5**.

The aggregation state of initial NPs can have an important effect on the final grain size of the consolidated sample (**Figure 6**). By varying the polyol during the NPs synthesis (by hydrolysis in a polyol method), different aggregation clustering can be achieved [9], from monodispersed NPs (reaction with diethylenglycol), ~10 NPs clusters (by using propanediol), and ~100 NPs clusters (prepared with ethanediol).

The size of the NPs was the same (~5 nm) in all clusters. The final grain sizes after consolidation exhibited the opposite tendency, that is, the largest grain size was found for the monodispersed sample. This points to the dependence of grain growth on surface diffusion; large

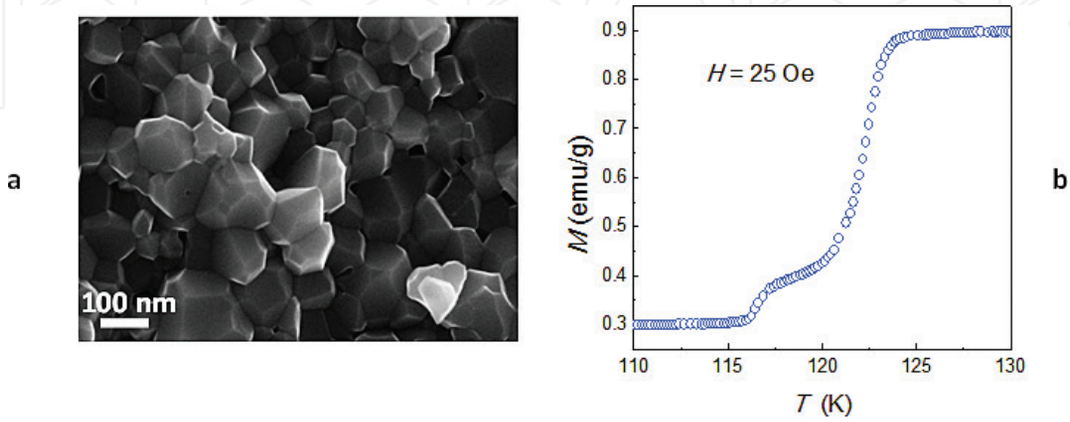

Figure 5. (a) SEM micrograph of magnetite consolidated by SPS at 750°C, 15 min and (b) magnetization measurements showing the Verwey transition (adapted from Ref. [49]).

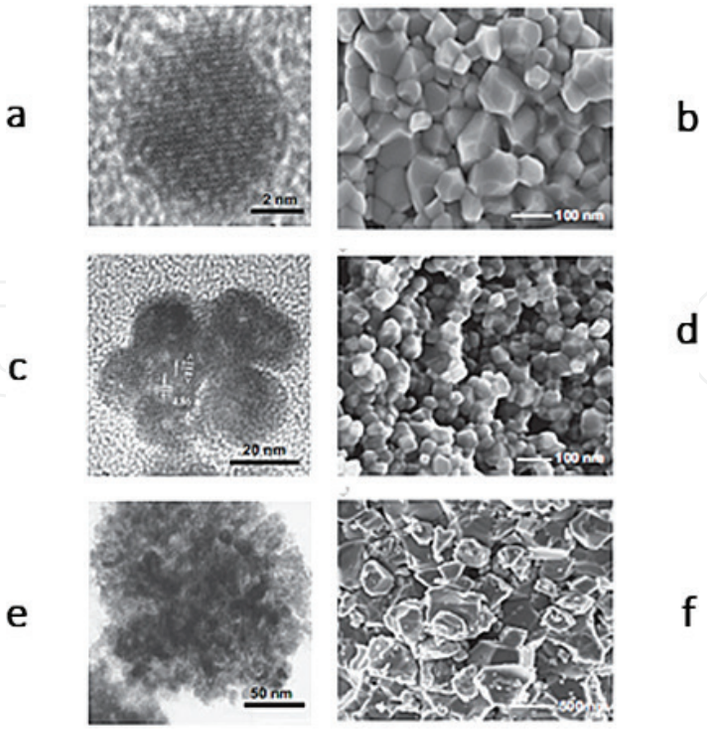

Figure 6. Polyol-synthesized NPs in different media: (a) diethylenglycol, (c) propanediol and (e) ethanediol; they led to SPS consolidated nanostructures (b), (d) and (f), respectively. Reprinted from Ref. [9] Copyright (2014), with permission from Elsevier.

clusters grow mainly through the cluster surface, while monodispersed NPs coalesce directly from their individual surface.

The importance of heating rate appears in **Figure 7**, where the nanostructure of a cobalt ferrite is shown for SPS processing at the same sintering temperature and times (2 min at 600°C followed by 5 min at 500°C), but with heating rates of 80°C/min, and 15°C/min [9]. Grain size is about 70 nm for the former, and 290 nm for the slow heating rate. This illustrates again the differences between surface and volume diffusion, as previously discussed.

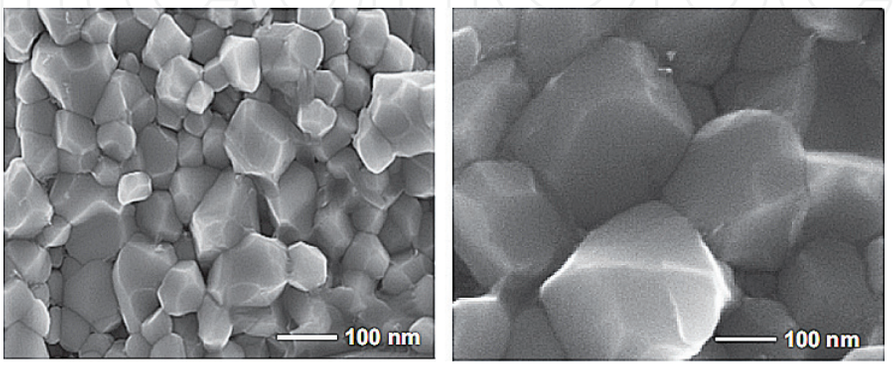

Figure 7. Co ferrite processed with different heating rates to reach the sintering temperature (600°C): left 80°C/min, and right 15°C/min. Reprinted from Ref. [9] Copyright (2014), with permission from Elsevier.

http://dx.doi.org/10.5772/68017

6. Consolidation of garnets

To the best of our knowledge, only hydrothermal, and more generally solvothermal, synthesis techniques may allow the more or less direct production of ferrites with the garnet structure. From a general point of view, dense oxide structures, namely crystalline cells containing a high number of atoms per unit volume like orthoferrite, garnet or hexaferrite cells, require a high activation energy to nucleate. This can be achieved by a postannealing treatment as explained above or by increasing the pressure during reaction solution heating.

If a consolidated phase is sought, then a SPS treatment can be applied by using the resulting precursors of a soft chemistry synthesis reaction. Yttrium iron garnet (YIG) can be prepared by a SPS treatment at 750°C for 15 min at 100 MPa from the precursors obtained from a polyol synthesis reaction [55], in big contrast with the typical parameters of the solid state reaction (1350°C for a few hours). Note that in these original shaping conditions, highly dense and ultrafine grained ceramics (**Figure 8**) were systematically obtained.

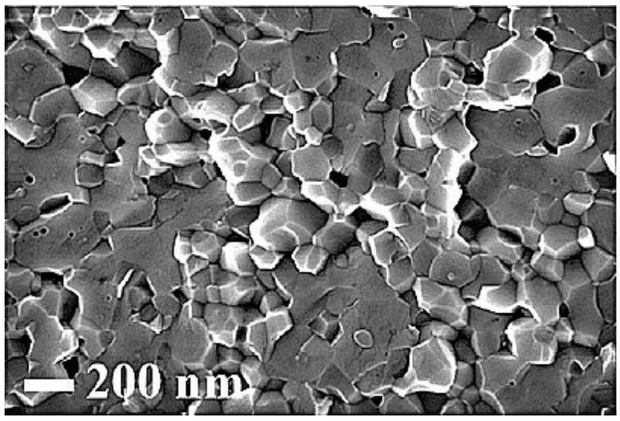

Figure 8. SEM micrograph of YIG obtained by polyol reaction + SPS treatment at 750°C, 15 min, 100 MPa. Reprinted with permission from Ref. [55], Copyright (2013) Wiley.

7. Synthesis of hexaferrites by SPS

Nanostructured hexaferrites can be synthesized by various methods such as sol-gel [56], coprecipitation [57], spray-drying and microemulsion [58], ball-milling [42], among others. However, the obtained products still need thermal posttreatments in the range of 800–1200°C to crystallize into hexagonal ferrites and get sintered. Different ways are used to minimize the grain growth before sintering. The annealed particles can be postmilled, resulting in smaller particles that in turn increase the density and decrease the sintering temperatures [59]. Another way is the containment of the particles in an amorphous glassy matrix before their annealing to form the desired phase while limiting its grain growth. One of the most impressive result is the crystallization of 57 nm M-ferrites obtained at 642°C with the addition of B_2O_3 glass vs 260 nm at 800°C with silica [60]. Besides, doping hexaferrites with Zn^{2+} and La^{3+} can also act as a grain growth inhibitor during annealing treatment [61].

Recently, the spark plasma sintering (SPS) method has brought an interesting alternative to synthesis/sinter hexaferrites and optimize their magnetic properties. Indeed, SPS is carried out at relatively low temperatures in a very short time of few minutes only, and additionally, it allows a convenient control of grain growth. Such observations apply to SrM-type hexaferrites prepared by the mechanical compounding method [62]. The resulting ceramics have a fine microstructure as illustrated in **Figure 9** [63].

SPS of $SrFe_{12}O_{19}$ at 1100°C for 5 min leads to a maximum density of 5.15 Mg/m^3, while the maximum density obtained by ordinary sintering at 1240°C for 2 h is only 4.83 Mg/m^3. In this case, the samples prepared by SPS showed half-sized grains (400 nm) and harder magnetic properties. The effect of SPS temperature and time on the density and magnetic properties of SrM ferrites was also significant. A high energy product $(BH)_{max}$ of 18.3 kJ/m^3 was found for such strontium hexaferrites [63]. Similarly, the sintering of Ba hexaferrites by SPS has also led to harder magnetic properties due to the limited grain growth: grains of ~100–150 nm by SPS vs 1.5–8 μm by conventional sintering [64].

SPS is not only useful to consolidate nanopowders, but it also promotes the chemical reaction of nanoparticles. Thus, SPS has been also used to complete the formation of nanostructured hexaferrites. SPS treatments were applied to a high-energy ball milled mixture of SrO and Fe_2O_3 precursors. The formation of 70 nm M-type strontium hexaferrites has been achieved at only 700°C, under 800 MPa [65]. XRD measurements revealed that such hexagonal ferrites crystallize from nucleation sites of $Fe_2Sr_2O_5$ that is an intermediate metastable phase formed at 600°C. In comparison with the simple annealing of the same ball milled precursors at 800°C, denser SPS treated samples show higher saturation magnetization (67 emu/g vs 58 emu/g) and lower coercivity (3.7 kOe vs 6.4 kOe) (**Figure 10(a)**) that are interesting features

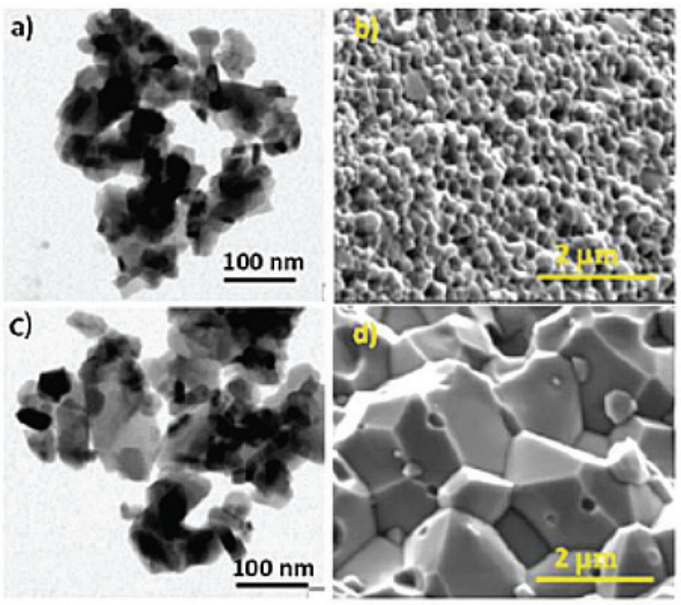

Figure 9. Ball-milled $SrFe_{12}O_{19}$ NPs annealed at different temperatures: (a) 700 and (c) 900°C and their related ceramics (b and d, respectively) resulting from SPS consolidation. Reprinted with permission from Ref. [63] Copyright (2016) American Chemical Society.

http://dx.doi.org/10.5772/68017

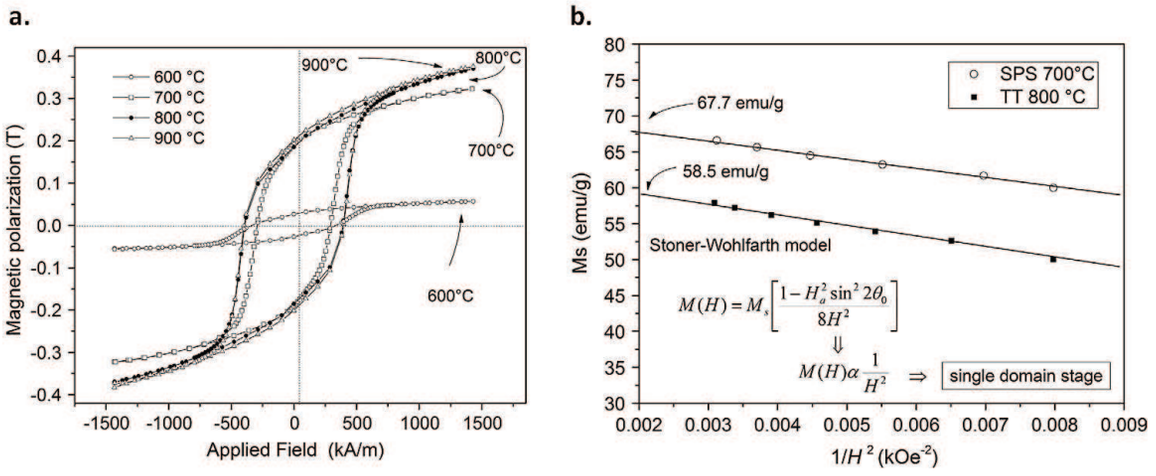

Figure 10. Sr-$Fe_{12}O_{19}$ prepared by SPS-assisted mecanosynthesis: (a) Hysteresis loops *M* vs *H* showing the effect of the SPS temperature on the magnetic properties and (b) comparison of the saturated magnetization *Ms* vs $1/H^2$ obtained after either SPS heating or conventional annealing. Republished with permission from Ref. [65] Copyright 2014, with permission through Copyright Clearance Center, Inc., Elsevier.

for recording media and electromagnetic fields wave absorption [66]. The linear M vs $1/H^2$ relationship–well fitted with the Stoner-Wohlfarth model of noninteracting single domains with uniaxial anisotropy–indicates that the decrease in coercivity is most likely due to the grain growth reduction below the single domain limit (**Figure 10(b)**). This result therefore contrasts with SPS-induced harder magnetic properties discussed earlier [62, 64], since reducing the grain growth in a range above or below the single domain limit has opposite effects on the coercivity.

The SPS-assisted synthesis of barium hexaferrites has also been demonstrated. $BaFe_{12}O_{19}$ was synthesized and sintered by SPS operated at 800°C for 10 min [67]. Interestingly, textured samples in nanobelt and nanorod microstructures were obtained showing an aspect ratio of 200 nm/several μm. Compared to textureless barium hexaferrites, the SPS-induced microstructures are characterized by higher Ms (65.5 emu/g) and lower coercivity H_c (1.4 kOe) reflecting an easier magnetic domain wall movement and/or a coherent magnetization rotation often observed for uniform microsized multidomains. It also reveals that the ultra-fast decomposition of $BaCO_3$ and $Fe(OH)_3$ precursors by SPS results in volume shrinkage leading to an accommodated nanostructure of barium hexaferrite. Furthermore, SPS can also produce hexaferrite bulk magnets of highly aligned single-magnetic domains without applying any magnetic field. This has been reported for the SPS compaction of $SrFe_{12}O_{19}$ nanoplatelets synthesized by supercritical hydrothermal flow method [68]. This effect is attributed to the highly aligned crystallites of the as-synthesized nanoplatelets together with the oriented crystal growth during SPS along the c-axis. Thus, SPS compacted samples at 950°C under 80 MPa for 2 min are composed of 80–100 nm nanocrystallites characterized by single-crystal-like magnetic properties, that is, high coercivity H_c (301 kA m^{-1}), M_s (69 A m^2 Kg^{-1}), M_r (59 A m^2 Kg^{-1}) and energy product *BH* (26 kJ m^{-3}).

As a final note, the SPS heating and pressing not only permits to decrease the crystallization/sintering temperatures of hexaferrites and to tailor their magnetic properties, but it also prevents the

formation of secondary phases such as α-Fe_2O_3 [68]. On the other hand, the reductive atmosphere in SPS can lead to hexaferrite decomposition and the subsequent magnetite formation (reduction of Fe^{3+} to Fe^{2+}) [69]. Nevertheless, a recent study has shown that such a Fe_3O_4 secondary phase can be suppressed by using protecting discs of aluminum oxide between the graphite mold and the samples [66].

8. Preparation of hybrid multiferroic composites by SPS

Multiferroic materials are commonly understood as those materials exhibiting at least two ferroic orders (i.e., ferroelectric and ferro- or ferrimagnetic orders) coupled in the same matrix, leading to a magneto-electric effect (ME), that is, a magnetic field induces a change in the electric response, or vice-versa. A strong interest has been aroused by such materials since many high-tech applications can be based on it. While ME effects may exist in a single phase material, the combination of two phases (i.e., a ferromagnet and a ferroelectric) in the same matrix (a "hybrid" multiferroic) has many advantages [70]. The ME effect can be tuned by varying the phase composition and interphase connectivity, which depend directly from the nanostructure.

The ME effects in hybrid multiferroics can be enhanced by increasing the contact area between the involved phases [10, 11]. In the case of homogeneously mixed grained composites, an effective way to do this is retaining the grain growth during the sintering process in order to keep the final grain size at nanoscale. It will increase the grain boundary surface and therefore the contact interface between different phases. The SPS technique has been demonstrated to be a very fast and efficient route to consolidate high-density bulk oxide ceramics, retaining grain sizes of the sintered materials at the scale of ~100 nm [7, 9, 14]. A very small grain size means a larger interphase surface and, therefore, a stronger ME coupling.

8.1. Spinel ferrite-based composites

The ferrite (ferromagnetic)/perovskite (ferroelectric) system has been mainly investigated. Nickel ferrite $NiFe_2O_4$/lead zirconate titanate PZT (or NFO/PZT for short) was investigated by Jiang from laboratory synthesized and commercial submicrometer sized precursors, respectively [71]. They obtained layered and homogeneously mixed multiferroic composites with submicrometer sized grains by using sintering temperatures between 900 and 1050°C, and pressures between 50 and 100 MPa (**Figure 11**). A certain degree of interphase diffusion between both phases was reported for this system. Although the last system was found to be suitable for practical applications because of their good ME properties and high density, the employment of lead in ceramics and other materials is nowadays discarded by most of the scientific community because of their impact on the environment.

To solve the lead problem, barium or strontium titanate is used, together with cobalt ferrite. In fact, the system $CFO_x/BTO_{(1-x)}$ has been widely researched. Hybrid multiferroics in this system have been prepared from commercial nanopowder reagents [72], commercial BTO and autocombustion synthesized CFO [73], at temperatures in the 1050°C range. A reduction in temperature (860°C) [74] was not enough to eliminate the interphase diffusion. The use

http://dx.doi.org/10.5772/68017

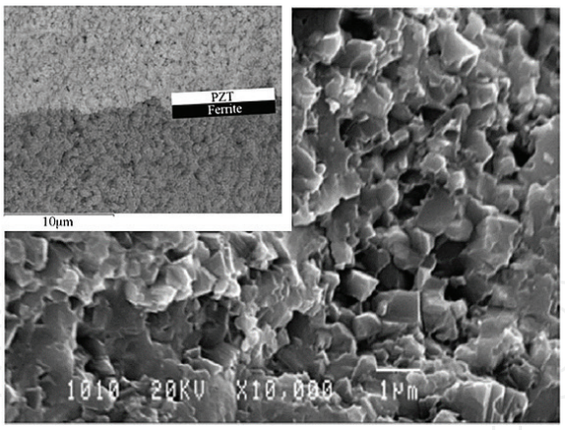

Figure 11. SEM image of homogeneous $NiFe_2O_4$ (NFO) ferrite/PZT composite revealing the grain size and morphology; the inset shows the interface between ferrite (NFO) and PZT (adapted from Ref. [71].

of starting NPs synthesized by coprecipitation and ball milling allowed [75] to eliminate the interdiffusion and improve the ME coupling coefficient.

The use of both initial NPs synthesized by soft chemistry, low temperatures in the 650°C, higher pressures (100 Mpa) and short sintering times (5 min), producing grain sizes in the 150 nm (see **Figure 12**), led to high ME coefficients and the absence of interdiffusion [76]. The use of Impedance Spectroscopy (i.e., the analysis of the electrical response of the material in a wide frequency range) exhibited three main components which can be associated [77] with the three corresponding interfaces: BTO-BTO, CFO-CFO, and CFO-BTO. Experiments as a function of frequency, temperature and applied magnetic field allowed establishing the polarization processes in the three interfaces.

In another work, Co-substituted Ni-Zn ferrite was synthesized using a nonconventional solid state reaction method and sintered by SPS at 850°C and 100 MPa [79]. This ferrite was used to make layered composites by pasting a layer of commercial PZT to the sintered pellet with silver epoxy. ME performances obtained with an optimized composition of NiCoZn ferrite/PZT bilayer were compared to those obtained with the same structure combining Terfenol-D and PZT. It was shown that the low piezomagnetic coupling performance of the ferrite (in comparison to the Terfenol-D) is balanced by a low compliance. Furthermore, they used Co-substituted Ni-Zn ferrite associated with PZT in a tri-layer structure to design a ME current sensor. This sensor can be readily used in the field of power electronic applications.

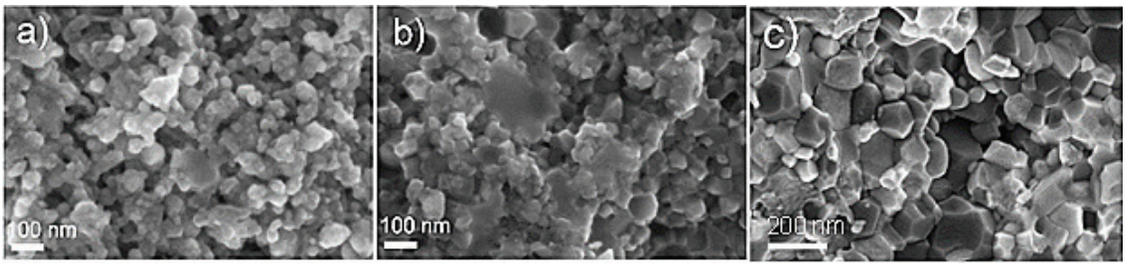

Figure 12. SEM micrographs of $CFO_x/BTO_{(1-x)}$ composites with (a) $x = 0.25$, (b) $x = 0.75$ and (c) $x = 0.50$, sintered at 650°C and 100 MPa for 5 min [78].

8.2. Other hybrid multiferroic composites

Additional efforts in this area have been reported recently in other type of ferrite-based hybrid multiferroics sintered by SPS. Bismuth ferrite (BFO) and BTO composites, sintered by SPS at temperatures around 800°C, and uniaxial pressures of 50 MPa have been prepared [80] from precursors with an average particle size of 1 μm leading to final microstructures with grain sizes all above 2 μm (**Figure 13**). Strontium hexaferrite and BTO-based hybrid multiferroics by SPS, starting from nanosized precursors purchased commercially, were investigated [81]. They were fabricated by SPS at a temperature of 900°C, a uniaxial pressure of 75 MPa and a sintering time of 3 min. These conditions (low T and short time) allowed final microstructures with grain sizes down to 200 nm and no interphase diffusion.

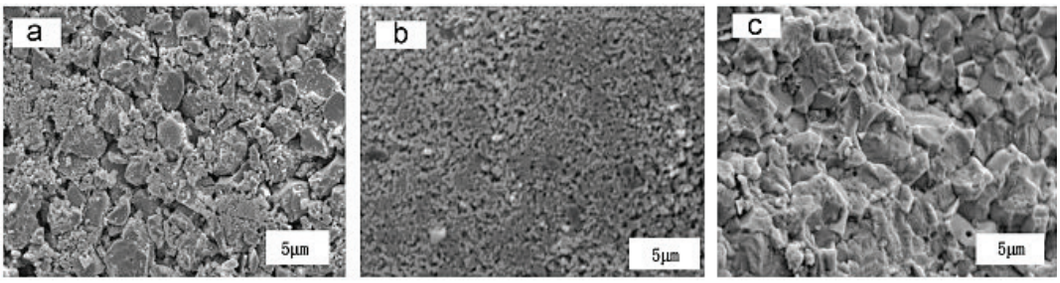

Figure 13. SEM images of 75% BFO-25%BTO at (a) 30 min mechanochemical synthesis, (b) 48 h of mechanochemical synthesis, and (c) after SPS sintering at 1000°C. Reprinted from Ref. [80] Copyright (2012), with permission from Elsevier [80].

8.3. General trends

The general trends in fabrication and characterization of hybrid multiferroics by SPS can be summarized as follows. It is possible to fabricate new high-density hybrid multiferroics by SPS, with enhanced dielectric, magnetic, and ME properties. Important variables such as the interphase diffusion, final microstructure of the sintered composites, as well as the nature and microstructural features of the starting precursors, all play a crucial role on the design of these materials. A fine grained high-density microstructure, with homogeneous average grain sizes down to 100 nm and well-defined grain boundaries, can be produced from soft-chemistry synthesized NPs. In order to retain the already formed phases of NPs and avoid interphase diffusion, short time and low temperature sintering is necessary. Sintering temperatures near to or higher than 1000°C are not recommended because a possible promotion of the interphase diffusion could result in a decrease of the dielectric constant.

9. Conclusions

At present, SPS appears to be the only practical method to produce high-density solids with grain size in the nanometer range. Additionally, SPS requires relatively lower temperatures and shorter times for densification compared to conventional sintering. In a very general way, final density increases with temperature, and grain size increases with time, so there

is a compromise. The solution can be to use a relatively high sintering temperature, with a high heating rate. Finally, a problem with oxides can be the strong reductive medium of SPS, which can lead to reduction to metallic impurities in an oxide. Again, this can be minimized by means of short sintering times.

Acknowledgements

RV acknowledges a sabbatical fellowship from DGAPA-UNAM Mexico.

Author details

Romain Breitwieser[1], Ulises Acevedo[1,2], Souad Ammar[1] and Raul Valenzuela[1,2]*

*Address all correspondence to: monjaras@unam.mx

1 ITODYS, Paris Diderot University, Sorbonne Paris Cité, Paris, France

2 Materials Research Institute, National Autonomous University of Mexico, Mexico City, Mexico

References

[1] Valenzuela R. Magnetic Ceramics. UK: Cambridge University Press; 2005. 312 p.

[2] Snelling EC. Soft Ferrites: Properties and Applications. USA: Ltd, Butterworth-Heinemann; 1988. 376 p.

[3] Vukovich DP. Overview of the World Magnet Supply: Llc, Alliance; 2013.

[4] Harris VG, Geiler A, Chen Y, Yoon SD, Wu M, Yang A, et al. Recent advances in processing and applications of microwave ferrites. Journal of Magnetism and Magnetic Materials. 2009;**321**(14):2035-47.

[5] Guimaraes AP. Principles of Nanomagnetism. Berlin: Springer, Verlag; 2009. 221 p.

[6] Guillon O, Gonzalez-Julian J, Dargatz B, Kessel T, Schierning G, Rathel J, et al. Field-assisted sintering technology/spark plasma sintering: Mechanisms, materials, and technology developments. Advanced Engineering Materials. 2014;**16**(7):830-849.

[7] Valenzuela R, Beji Z, Herbst F, Ammar S. Ferromagnetic resonance behavior of spark plasma sintered Ni-Zn ferrite nanoparticles produced by a chemical route. Journal of Applied Physics. 2011;**109**(7):07A329.

[8] Nygren Z, Shen M. Microstructural prototyping of ceramics by kinetic engineering: Applications of spark plasma sintering. Chemical Record. 2005;**5**(3):173-184.

[9] Gaudisson T, Artus M, Acevedo U, Herbst F, Nowak S, Valenzuela R, et al. On the microstructural and magnetic properties of fine-grained $CoFe_2O_4$ ceramics produced by combining polyol process and spark plasma sintering. Journal of Magnetism and Magnetic Materials. 2014;**370**:87-95.

[10] Ma J, Hu J, Li Z, Nan CW. Recent progress in multiferroic magnetoelectric composites: From bulk to thin films. Advanced Materials. 2011;**23**(9):1062-1087.

[11] Schileo G. Recent developments in ceramic multiferroic composites based on core/shell and other heterostructures obtained by sol–gel routes. Progress in Solid State Chemistry. 2013;**41**(4):87-98.

[12] Gubin SP, Koksarov YA, Khomutov GB, Yurkov GY. Magnetic nanoparticles: Preparation, structure and properties. Russian Chemical Reviews. 2005;**74**(6):489-520

[13] Artus M, Tahar LB, Herbst F, Smiri L, Villain, Yaacoub FN, et al. Size-dependent magnetic properties of $CoFe_2O_4$ nanoparticles prepared in polyol. Journal of Physics: Condensed Matter. 2011;**23**(50):506001.

[14] Acevedo U, Gaudisson T, Ortega-Zempoalteca R, Nowak S, Ammar S, Valenzuela R. Magnetic properties of ferrite-titanate nanostructured composites synthesized by the polyol method and consolidated by spark plasma sintering. Journal of Applied Physics. 2013;**113**(17):17B519.

[15] Munir Z, Anselmi-Tamburini U, Ohyanagi M. The effect of electric field and pressure on the synthesis and consolidation of materials: A review of the spark plasma sintering method. Journal of Materials Science. 2006;**41**(3):763-777.

[16] Garay J, Glade S, Anselmi-Tamburini U, Asoka-Kumar P, Munir Z. Electric current enhanced defect mobility in Ni_3Ti intermetallics. Applied Physics Letters. 2004;**85**(4):573-575.

[17] Shen Z, Johnsson M, Zhao Z, Nygren M. Spark plasma sintering of alumina. Journal of the American Ceramic Society. 2002;**85**(8):1921-1927.

[18] Yu W, Falkner J, Yavuz C, Colvin V. Synthesis of monodisperse iron oxide nanocrystals by thermal decomposition of iron carboxylate salts. Chemical Communications. 2004(20):2306-2307.

[19] Soundararajan D, Kim K. Synthesis of $CoFe_2O$ magnetic nanoparticles by thermal decomposition. Journal of Magnetics. 2014;**19**(1):5-9.

[20] Naseri M, Saion E, Ahangar H, Shaari A, Hashim M. Simple synthesis and characterization of cobalt ferrite nanoparticles by a thermal treatment method. Journal of Nanomaterials. 2010;**2010**: 907686-94 .

[21] Chinie AM, Stefan A, Georgescu S. Synthesis by a citrate sol-gel method and characterization of Eu^{3+} doped yttrium aluminium garnet nanocrystals. Romanian Reports in Physics. 2005;**57**(3):412-417.

[22] Lai Z, Xu G, Yalin Z. Microwave assisted low temperature synthesis of MnZn ferrite nanoparticles. Nanoscale Research Letters. 2007;**2**(1):40-43.

[23] Kalyani S, Sangeetha J, Philip J. Microwave assisted synthesis of ferrite nanoparticles: Effect of reaction temperature on particle size and magnetic properties. Journal of Nanoscience and Nanotechnology. 2015;**15**(8):5768-5774.

[24] Daou T, Pourroy G, Begin-Colin S, Greneche J, Ulhaq-Bouillet C, Legare P, et al. Hydrothermal synthesis of monodisperse magnetite nanoparticles. Chemistry of Materials. 2006;**18**(18):4399-4404.

[25] Koseoglu Y, Alan F, Tan M, Yilgin R, Ozturk M. Low temperature hydrothermal synthesis and characterization of Mn doped cobalt ferrite nanoparticles. Ceramics International. 2012;**38**(5):3625-3634.

[26] Wang J, Ren F, Yi R, Yan A, Qiu G, Liu X. Solvothermal synthesis and magnetic properties of size-controlled nickel ferrite nanoparticles. Journal of Alloys and Compounds. 2009;**479**(1-2):791-796.

[27] Yanez-Vilar S, Sanchez-Andujar M, Gomez-Aguirre C, Mira J, Senaris-Rodriguez M, Castro-Garcia S. A simple solvothermal synthesis of MFe_2O_4 (M = Mn, Co and Ni) nanoparticles. Journal of Solid State Chemistry. 2009;**182**(10):2685-2690.

[28] Xu H, Zeiger B, Suslick K. Sonochemical synthesis of nanomaterials. Chemical Society Reviews. 2013;**42**(7):2555-2567.

[29] Abedini A, Daud A, Hamid M, Othman N, Saion E. A review on radiation-induced nucleation and growth of colloidal metallic nanoparticles. Nanoscale Research Letters. 2013;**8:1-10**.

[30] Abedini A, Daud A, Hamid M, Othman N. Radiolytic formation of Fe_3O_4 nanoparticles: Influence of radiation dose on structure and magnetic properties. Plos One. 2014;**9**(3):e90055.

[31] Yadav TP, Yadav RM, Singh DP. Mechanical milling: A top down approach for the synthesis of nanomaterials and nanocomposites. Journal of Nanoscience and Nanotechnology. 2012;**2**(3):22-48.

[32] Gaffet E, Abdellaoui M, Malhourous-Gaffet N. Formation of nanostructured materials induced by mechanical processings (overview). Materials Transactions JIM. 1995;**36**:198-209.

[33] Tan O, Cao W, Hu Y, Zhu W. Nanostructured oxides by high-energy ball milling technique: Application as gas sensing materials. Solid State Ionics. 2004;**172**(1-4):309-316.

[34] Gorrasi G, Sorrentino A. Mechanical milling as a technology to produce structural and functional bio-nanocomposites. Green Chemistry. 2015;**17**(5):2610-2625.

[35] Ullah M, Ali M, Abd Hamid S. Surfactant-assisted ball milling: A novel route to novel materials with controlled nanostructure—A review. Reviews on Advanced Materials Science. 2014;**37**(1-2):1-14.

[36] Cruz-Franco B, Gaudisson T, Ammar S, Bolarin-Miro A, Sanchez de Jesus F, Mazaleyrat F, et al. Magnetic properties of nanostructured spinel ferrites. IEEE Transactions on Magnetics. 2014;**50**(4):2800106.

[37] Ammar S, Helfen A, Jouini N, Fievet F, Rosenman I, Villain F, et al. Magnetic properties of ultrafine cobalt ferrite particles synthesized by hydrolysis in a polyol medium. Journal of Materials Chemistry. 2001;**11**(1):186-92.

[38] Beji Z, Smiri L, Yaacoub N, Greneche J, Menguy N, Ammar S, et al. Annealing effect on the magnetic properties of polyol-made Ni-Zn ferrite nanoparticles. Chemistry of Materials. 2010;**22**(4):1350-66.

[39] Ammar S, Jouini N, Fievet F, Beji Z, Smiri L, Moline P, et al. Magnetic properties of zinc ferrite nanoparticles synthesized by hydrolysis in a polyol medium. Journal of Physics-Condensed Matter. 2006;**18**(39):9055-9069.

[40] Hu P, Yang H, Pan D, Wang H, Tian J, Zhang S, et al. Heat treatment effects on microstructure and magnetic properties of Mn-Zn ferrite powders. Journal of Magnetism and Magnetic Materials. 2010;**322**(1):173-177.

[41] Gonzalez F, Miro A, De Jesus F, Escobedo C, Ammar S. Mechanism and microstructural evolution of polyol mediated synthesis of nanostructured M-type $SrFe_{12}O_{19}$. Journal of Magnetism and Magnetic Materials. 2016;**407**:188-94.

[42] Sanchez-De Jesus F, Bolarin-Miro A, Cortes-Escobedo C, Valenzuela R, Ammar S. Mechanosynthesis, crystal structure and magnetic characterization of M-type $SrFe_{12}O_{19}$. Ceramics International. 2014;**40**(3):4033-4038.

[43] Sanchez-De Jesus F, Cortes C, Valenzuela R, Ammar S, Boarin-Miro A. Synthesis of $Y_3Fe_5O_{12}$ (YIG) assisted by high-energy ball milling. Ceramics International. 2012;**38**(6):5257-5263.

[44] Wang M, Zhu X, Wei X, Zhang L, Yao X. Preparation and annealing process of $Y_3Fe_5O_{12}$ by sol-gel method. Ferroelectrics. 2001;**264**(1-4):1907-1912.

[45] Yamamoto S, Horie S, Tanamachi N, Kurisu H, Matsuura M. Fabrication of high-permeability ferrite by spark-plasma-sintering method. Journal of Magnetism and Magnetic Materials. 2001;**235**(1-3):218-222.

[46] Sun J, Li J, Sun G, Qu W. Synthesis of dense NiZn ferrites by spark plasma sintering. Ceramics International. 2002;**28**(8):855-888.

[47] Gaudisson T, Beji Z, Herbst F, Nowak S, Ammar S, Valenzuela R. Ultrafine grained high density manganese zinc ferrite produced using polyol process assisted by spark plasma sintering. Journal of Magnetism and Magnetic Materials. 2015;**387**:90-95.

[48] Valenzuela R, Ammar S, Nowak S, Vazquez G. Low field microwave absorption in nanostructured ferrite ceramics consolidated by spark plasma sintering. Journal of Superconductivity and Novel Magnetism. 2012;**25**(7):2389-2393.

[49] Gaudisson T, Vazquez-Victorio G, Banobre-Lopez M, Nowak S, Rivas J, Ammar S, et al. The Verwey transition in nanostructured magnetite produced by a combination of chimie douce and spark plasma sintering. Journal of Applied Physics. 2014;**115**(17):17E117.

[50] Ortega-Zempoalteca R, Flores-Arias Y, Vazquez-Victorio G, Gaudisson T, Ammar S, Vargas-Osorio Z, et al. The effects of spark plasma sintering consolidation on the ferromagnetic resonance specta (FMR) of Ni-Zn ferrites. Physica Status Solidi A. 2014;**211**:1062-1066.

[51] Ammar S et al, Unpublished results.

[52] Verwey EJW. Electronic conduction of magnetite (Fe_3O_4) and its transition point at low temperatures. Nature. 1939;**144**:327-328.

[53] Senn MS, Wright JP, Attfield JP. Charge order and three-site distortions in the Verwey structure of magnetite. Nature. 2012;**481**:173-176.

[54] Skumryev V, Blythe HJ, Cullen J, Coey JMD. AC susceptibility of a magnetite crystal. Journal of Magnetism and Magnetic Materials. 1999;**196-197**:515-517.

[55] Gaudisson T, Acevedo U, Nowak S, Yaacoub N, Greneche J-M, Ammar S, et al. Combining soft chemistry and spark plasma sintering to produce highly dense and finely grained soft ferrimagnetic $Y_3Fe_5O_{12}$ (YIG) ceramics. Journal of the American Ceramic Society. 2013;**96**(10):3094-3049.

[56] X. Liu WZ, S. Yang, Z. Yu, B. Gu, Du Y. Structure and magnetic properties of La^{3+}-substituted strontium hexaferrite particles prepared by sol–gel method. Physica Status Solidi A. 2002;**193**(2):314-319.

[57] Ataie A, Heshmati-Manesh S. Synthesis of ultra-fine particles of strontium hexaferrite by a modified co-precipitation method. Journal of European Ceramic Society. 2001;**21**(10):1951-1955.

[58] Chen D-H, Chen Y-Y. Synthesis of strontium ferrite ultrafine particles using microemulsion processing. Journal of Colloid and Interface Science. 2001;**236**(1):41-46.

[59] Naiden EP, Itin VI, Terekhova OG. Mechanochemical modification of the phase diagrams of hexagonal oxide ferrimagnets. Technical Physics Letters. 2003;**29**(11):889-891.

[60] Kurisu S, Kubo O, editors. Ferrites. Tokyo and Kyoto, Japan: ICF6; 1992.

[61] Taguchi H, Takeishi V, Suwa K, Masuzawa K, Minachi Y. High energy ferrite magnets. Journal de Physique IV France. 1997;**7**(C1):311-312.

[62] Obara G, Yamamoto H, Tani M, Tokita M. Magnetic properties of spark plasma sintering magnets using fine powders prepared by mechanical compounding method. Journal of Magnetism and Magnetic Materials. 2002;**239**(1-3):464-467.

[63] Boda SK, Thrivikraman G, Panigrahy B, Sarma DD, Basu B. Competing roles of substrate composition, microstructure, and sustained strontium release in directing osteogenic differentiation of hMSCs. ACS Applied Materials & Interfaces. 2016;**8**:31567-31573.

[64] Ovtar S, Le Gallet S, Minier L, Millot N, Lisjak D. Control of barium ferrite decomposition during spark plasma sintering: Towards nanostructured samples with anisotropic magnetic properties. Journal of the European Ceramic Society. 2014;**34**:337-346.

[65] Bolarin AM, Sanchez De Jesus F, Cortes-Escobedo CA, Díaz-De la Torre S, Valenzuela R. Synthesis of M-type $SrFe_{12}O_{19}$ by mechanosynthesis assisted by spark plasma sintering. Journal of Alloys and Compounds. 2014;**643**(S1):S226-S230.

[66] Dehghan R, Seyyed Ebrahimi SA. Optimized nanocrystalline strontium hexaferrite prepared by applying a methane GTR process on a conventionally synthesized powder. Journal of Magnetism and Magnetic Materials. 2014;**368**:234-239.

[67] Zhao W-Y, Zhang Q-J, Tang X-F, Cheng H-B, Zhai P-C. Nanostructural M-type barium hexaferrite synthesized by spark plasma sintering method. Journal of Applied Physics. 2006;**99**(8):08E909.

[68] Saura-Muzquiz M, Granados-Miralles C, Stingaciu M, Bojesen ED, Li Q, Song J, et al. Improved performance of $SrFe_{12}O_{19}$ bulk magnets through bottom-up nanostructuring. Nanoscale. 2016;**8**:2857-2866.

[69] Stingaciu M, Topole M, McGuiness P, Christensen M. Magnetic properties of ball-milled $SrFe_{12}O_{19}$ particles consolidated by spark-plasma sintering. Nature, Scientific Reports. 2015;5:14112.

[70] Spaldin NA, Fiebig M. The renaissance of magnetoelectric multiferroics. Materials Science. 2005;**309**(5733):391-392.

[71] Jiang QH, Shen ZJ, Zhoua JP, Shia Z, Nan CW. Magnetoelectric composites of nickel ferrite and lead zirconnate titanate prepared by spark plasma sintering. Journal of the European Ceramic Society. 2007;**27**(1):279-284.

[72] Stingaciu M, Kremer RK, Lemmens P, Johnsson M. Magnetoresistivity in $CoFe_2O_4$-$BaTiO_3$ composites produced by spark plasma sintering. Journal of Applied Physics. 2011;**110**(4):044903.

[73] Liu Y, Ruan X, Zhu B, Chen S, Lu Z, Shi J, et al. $CoFe_2O_4/BaTiO_3$ Composites via spark plasma sintering with enhanced magnetoelectric coupling and excellent anisotropy. Journal of the American Ceramic Society. 2011;**94**(6):1695-1697.

[74] Ghosh D, Han H, Nino JC, Subhash G, Jones JL. Synthesis of $BaTiO_3$ 20wt%$CoFe_2O_4$ nanocomposites via spark plasma sintering. Journal of the American Ceramic Society. 2012;**95**(8):2504-2509.

[75] Etier M, Schmitz-Antoniak C, Salamon S, Trivedi H, Gao Y, Nazrabi A, et al. Magnetoelectric coupling on multiferroic cobalt ferrite–barium titanate ceramic composites with different connectivity schemes. Acta Materialia. 2015;**15**:1-9.

[76] Lopez Noda R, Acevedo Salas U, Gaudisson T, Piñar FC, Ammar S, Valenzuela R. Magnetoelectric coupling in $BaTiO_3$–$CoFe_2O_4$ nanocomposites studied by impedance spectroscopy under magnetic field. IEEE Transactions on Magnetics. 2014;**50**(11):8002304.

[77] Acevedo U, Lopez-Noda R, Breitwieser R, Calderon F, Ammar S, Valenzuela R. An impedance spectroscopy study of magnetodielectric coupling in $BaTiO_3$-$CoFe_2O_4$ nanostructured multiferroics. AIP Advances. 2017;**7**:055813.

[78] Acevedo U, Unpublished results.

[79] Loyau V, Morin V, Chaplier G, LoBue M, Mazaleyrat F. Magnetoelectric effect in layered ferrite/PZT composites. Study of the demagnetizing effect on the magnetoelectric behavior. Journal of Applied Physics. 2015;**117**(18):184102.

[80] Dai Z, Akishige Y. Electrical properties of $BiFeO_3$–$BaTiO_3$ ceramics fabricated by mechanochemical synthesis and spark plasma sintering. Materials Letters. 2012;**88**:36-39.

[81] Stingaciu M, Reuvekamp PG, Tai C-W, Kremer RK, Johnsson M. The magnetodielectric effect in $BaTiO_3$–$SrFe_{12}O_{19}$ nanocomposites. Journal of Materials Chemistry C. 2014;**2**:325-330.

IntechOpen